Supplementary Information

Decoupled Rigid–Flexible Synergistic Assembly in Robust Hydrogen-Bonded Organic Frameworks for Directional Proton Transport

Zhongxin Wei,[†a] Jiawei Jiang,[†a] Zizhu Yao,[a,b] Chulong Liu,[*a] Shengchang Xiang,[a] and Zhangjing Zhang[*a]

[a] *Fujian Provincial Key Laboratory of Polymer Materials, College of Chemistry and Materials Science, Fujian Normal University, 32 Shangsan Road, Fuzhou 350007, PR China*

[b] *State Key Laboratory of Structural Chemistry, Fujian Institute of Research on the Structure of Matter, Chinese Academy of Sciences, Fuzhou 350002, People's Republic of China.*

† These authors contributed equally to this work.

* Corresponding authors

E-mail: liucl@fjnu.edu.cn (Liu, C.); zzhang@fjnu.edu.cn (Zhang, Z.)

Experimental section

Materials and methods

All reagents and solvents are commercially available and directly used without further purification. ^{1}H NMR were performed on Bruker Advance III 400 MHz. The Fourier transform infrared (FT-IR) spectra (KBr pellets) were recorded in the range of 400–4000 cm^{-1} on a Thermo Nicolet 5700 spectrograph. Thermogravimetric analyses (TGA) were performed with METTLER TGA/SDTA 851 thermal analyzer with a heating rate of 10 °C min^{-1} from 30 to 600 °C under N_2 atmosphere. Powder X-ray diffraction (PXRD) patterns were recorded using Cu Kα radiation (λ = 1.5418 Å) on a PANalytical X'Pert[3] powder diffractometer with a vacuum apparatus at 40 kV and 40 mA. The water adsorption test was conducted on the Biesde Instrument BSD-VVS.

Single-crystal X-ray structural analysis

Data collection and structural analyses were performed on an Agilent Technologies Super Nova single crystal diffractometer equipped with graphit monochromatic Cu Ka radiation (λ = 1.5418 Å). We have fixed the 405 nm laser inside the single crystal diffractometer to ensure that the light source can be directed at the single crystal in situ. Using Olex2,[1] the structures were solved with the ShelXL[2] structure solution program using charge flipping and refined with the ShelXL refinement package using least-squares minimization. All nonhydrogen atoms were refined with anisotropic displacement parameters. The hydrogen atoms bonded to framework atoms were placed at idealized positions and refined using a riding model. The lattice water molecule in HOF-FJU-356 was refined with partial occupancy (0.5 per formula unit).

Proton conductivity measurement

Proton conductivity measurements and impedance analysis of the single-crystal samples were conducted using a two-probe configuration with a Solartron SI 1260 Impedance/Gain-Phase Analyzer and a 1296 Dielectric Interface Impedance Analyzer over a frequency range of 1 Hz to 1 MHz. The relative humidity and temperature environment are precisely controlled by the constant temperature and humidity chamber SMA-100PF (temperature: 0 °C to +150 °C; humidity: 20% to 98% RH). Before each test, the samples are placed in the target temperature and humidity for 30 min to reach a balanced state, ensuring that the framework can achieve a stable state corresponding to the set humidity.

Proton conductivity was calculated using the following equation:

$$\sigma = \frac{L}{RS} \qquad (1)$$

Where L and S are the length (cm) and cross-sectional area (cm^2) of the samples, respectively, and R is the bulk resistance (Ω) of the sample, which was extracted directly from the impedance

plots. The activation energy (E_a) for the material's conductivity was estimated from the following equation:

$$\sigma T = \sigma_0 exp(-\frac{E_a}{k_B T}) \quad (2)$$

where σ is the proton conductivity, σ_0 is the preexponential factor, k_B is the Boltzmann constant, and T is the temperature.

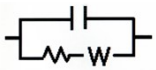

(3)

ZView software was used to extrapolate impedance data results by means of an equivalent circuit simulation to complete the Nyquist plot and obtain the resistance values. The selection of the equivalent circuit model followed the criteria suggested by Ciucci, which should be information-maximizing and consistent with the practical implications of physics.

Synthesis of 4,4',4'',4'''-(ethene-1,1,2,2-tetrayl)tetraaniline (ETTA)

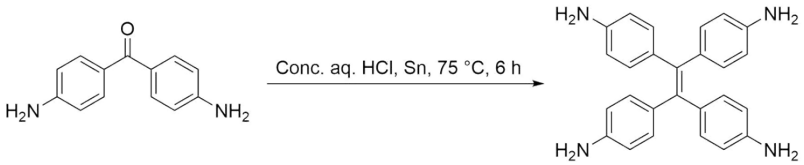

Scheme S1. Synthesis of 4,4',4'',4'''-(ethene-1,1,2,2-tetrayl)tetraaniline

4,4',4'',4'''-(Ethene-1,1,2,2-tetrayl)tetraaniline (ETTA) was synthesized according to a reported literature procedure with slight modifications (Scheme S1).[3] Briefly, 4,4'-diaminobenzophenone (1.6 g, 7.6 mmol) was dissolved in concentrated hydrochloric acid (70 mL) with heating and stirring in a round-bottom flask. To this solution, tin powder (6.0 g, 50.6 mmol) was added, and the reaction mixture was stirred at 75 °C for 6 h. After completion, the mixture was cooled to room temperature and then placed in an ice bath. Subsequently, the mixture was carefully neutralized to pH > 13 by the gradual addition of NaOH pellets with vigorous stirring, resulting in the formation of a substantial precipitate. The precipitate was collected by vacuum filtration and thoroughly washed with deionized water (3 × 50 mL). The crude solid was then dissolved in methanol, and the insoluble residues were removed by filtration. The filtrate was concentrated under reduced pressure to afford the crude product. Further purification was achieved by silica gel column chromatography using ethyl acetate as the eluent. The fractions containing the desired product were combined and concentrated, and the resulting solid was dried under vacuum to yield ETTA as a yellow powder. (0.51 g, 34.5% yield). ^{1}H NMR (400 MHz, DMSO-d_6) δ 6.57 (d, J = 8.4 Hz, 8H), 6.26 (d, J = 8.4 Hz, 8H), 4.85 (brs, 8H).

Growth of Single Crystals

Synthesis of HOF-FJU-356. An aqueous solution (20 mL) of methanedisulfonic acid (H_2MDS, 88.1 mg, 0.50 mmol) was added to a methanol solution (40 mL) of ETTA (78.5 mg, 0.20 mmol). The resulting mixture was then allowed to stand undisturbed for 1 d at room temperature, resulting in the formation of pale purple transparent crystals of HOF-FJU-356 with a yield of 87%. IR (KBr, cm^{-1}): 3451 (m), 2937 (s), 2613 (m), 1613 (m), 1573 (m), 1509 (s), 1423 (w), 1383 (w), 1231 (s), 1070 (m), 1012 (s), 795 (m), 770 (m).

Synthesis of HOF-FJU-357. An aqueous solution (20 mL) of ethane-1,2-disulfonic acid (H_2EDS, 95.1 mg, 0.50 mmol) was added to a methanol solution (40 mL) of ETTA (78.5 mg, 0.20 mmol). The resulting mixture was then allowed to stand undisturbed for 1 d at room temperature, resulting in the formation of pale green transparent rod-shaped crystals of HOF-FJU-357 with a yield of 92%. IR (KBr, cm^{-1}): 3421 (m), 2946 (s), 2641 (m), 1608 (m), 1559 (m), 1513 (s), 1432 (w), 1241 (s), 1169 (s), 1111 (m), 1025 (s), 836 (m), 773 (m).

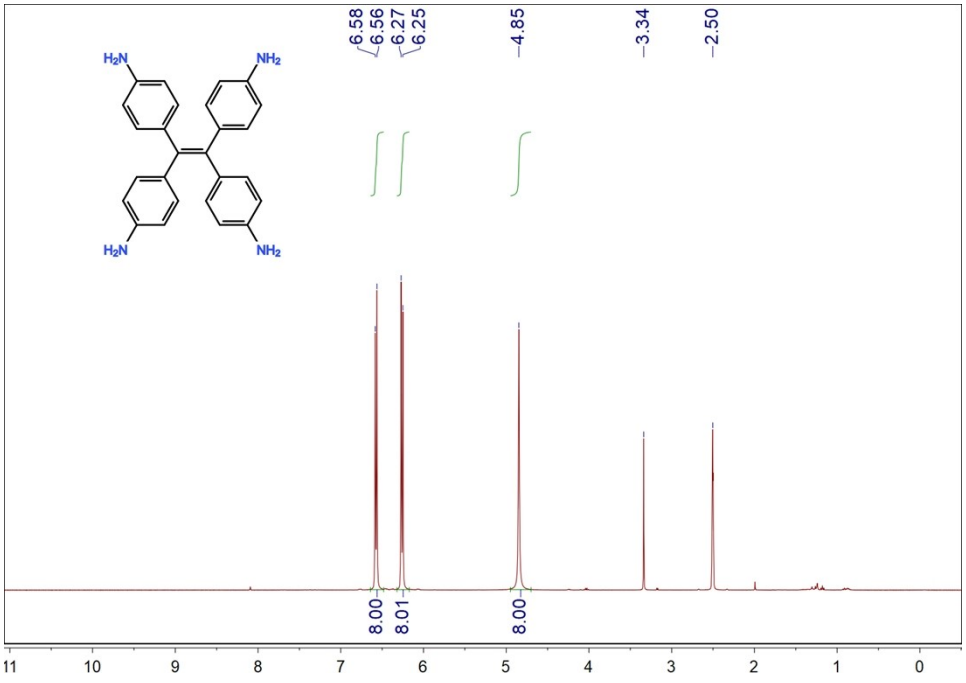

Fig. S1. ^{1}H NMR spectrum (400 MHz, DMSO-d_6) of ETTA.

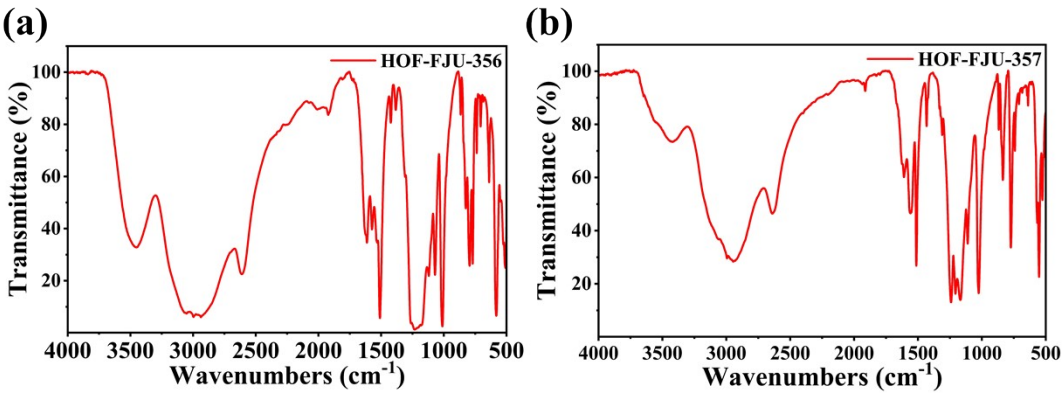

Fig. S2. FT-IR spectra of (a) HOF-FJU-356 and (b) HOF-FJU-357.

Crystal data and structure

Table S1. Crystallographic data and structural refinement summary

Identification code	HOF-FJU-356	HOF-FJU-357
CCDC	2497637	2497638
Empirical formula	$C_{28}H_{33}N_4O_{12.5}S_4$	$C_{30}H_{44}N_4O_{16}S_4$
Formula weight	753.82	884.93
Temperature/K	292.61	100.00
Crystal system	monoclinic	triclinic
Space group	$P2_1$	$P\bar{1}$
a/Å	12.9564(3)	10.5109(2)
b/Å	10.3265(2)	12.7386(5)
c/Å	15.4288(4)	14.3882(6)
α/°	90	88.137(3)
β/°	113.602(3)	89.436(3)
γ/°	90	79.054(3)
Volume/Å^3	1891.60(9)	1890.43(12)
Z	2	2
ρ_{calc}/g cm^{-3}	1.323	1.484
μ/mm^{-1}	2.991	2.850
F(000)	786.0	888.0
Crystal size/mm^3	0.22 × 0.1 × 0.03	0.37 × 0.04 × 0.01
Radiation	Cu $K\alpha$ (λ = 1.54184)	Cu $K\alpha$ (λ = 1.54184)
Reflections collected	9704	19292
Independent reflections	R_{int} = 0.0465, R_{sigma} = 0.0471	R_{int} = 0.0559, R_{sigma} = 0.0560
Data/restraints/parameters	5387/23/467	7254/9/455
Goodness-of-fit on F^2	1.057	0.889
Final R indexes [$I >= 2\sigma(I)$][(a)]	R_1 = 0.0627, wR_2 = 0.1737	R_1 = 0.1384, wR_2 = 0.3890
Final R indexes [all data][(a)]	R_1 = 0.0699, wR_2 = 0.1828	R_1 = 0.1451, wR_2 = 0.3921
Largest diff. peak/hole / e Å^{-3}	0.60/-0.57	2.32/-0.97

(a) $R_1 = \Sigma \, ||F_O|-|F_C|| \, / \, \Sigma \, |F_O|$; $wR_2 = [\Sigma \, w(|F_O|^2 - |F_C|^2)^2 \, / \, \Sigma \, w(F_O^2)^2]^{1/2}$

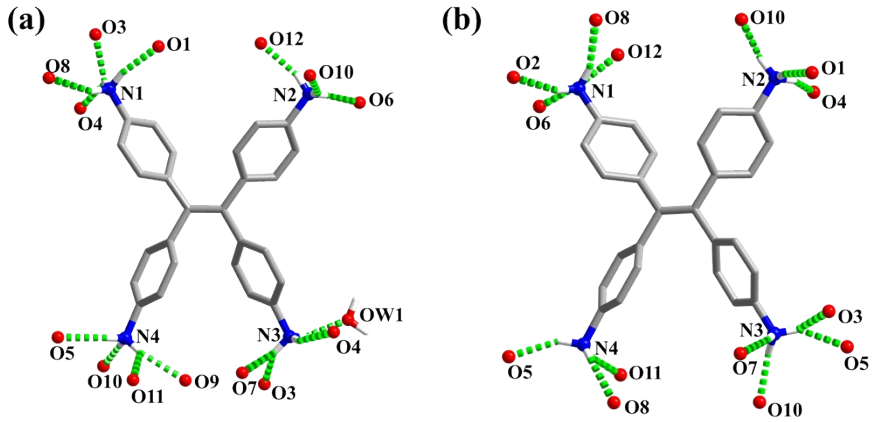

Fig. S3. The hydrogen bonding patterns in (a) HOF-FJU-356 and (b) HOF-FJU-357.

Table S2. Partial hydrogen bond parameters.

D···A / Å			
HOF-FJU-356		**HOF-FJU-357**	
N1-H1···O8	2.878	N1-H1···O2	2.749
N1-H2···O4	2.943	N1-H2···O6	2.813
N1-H2···O3	2.865	N1-H2···O12	2.859
N1-H3···O1	2.779	N1-H3···O8	2.84
N2-H4···O12	2.819	N2-H4···O10	2.833
N2-H5···O6	2.738	N2-H5···O4	2.885
N2-H6···O10	2.865	N2-H6···O1	2.893
N3-H7···O7	2.790	N3-H7···O10	2.825
N3-H7···O3	2.945	N3-H8···O5	2.984
N3-H8···OW1	2.825	N3-H8···O3	2.857
N3-H9···O4	3.117	N3-H9···O7	2.786
N4-H10···O5	2.775	N4-H10···O5	2.868
N4-H11···O10	2.936	N4-H11···O11	2.785
N4-H12···O9	2.923	N4-H12···O8	2.816
N4-H12···O11	2.867		

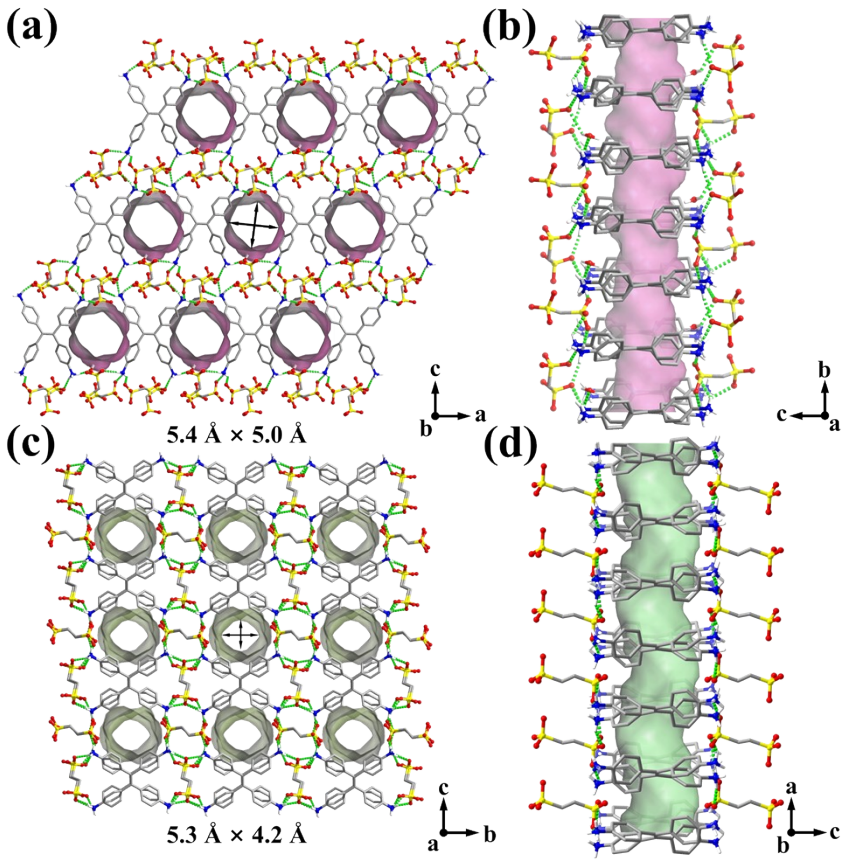

Fig. S4. Schematic representations of the pore structures of (a,b) HOF-FJU-356 and (c,d) HOF-FJU-357.

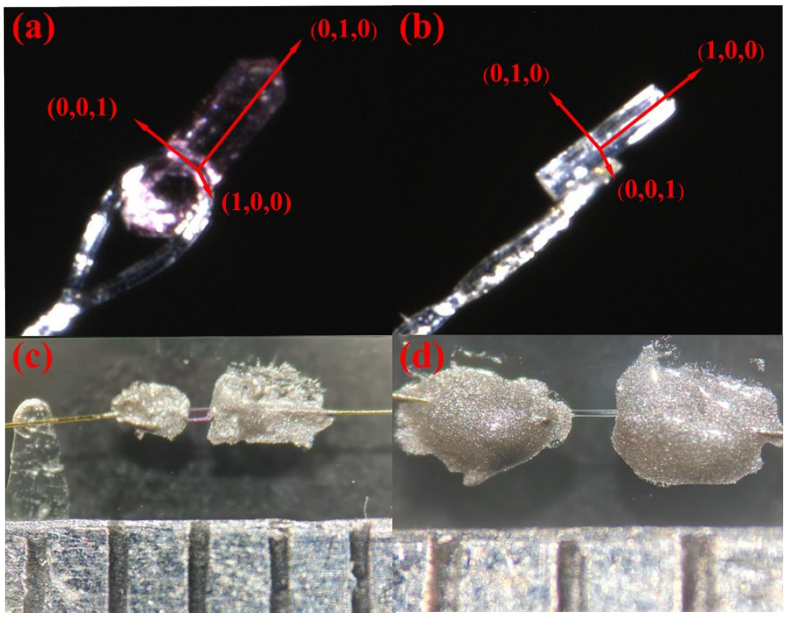

Fig. S5. Single crystal of (a) HOF-FJU-356 and (b) HOF-FJU-357 on the X-ray diffractometer and the diffractions corresponding to each direction of the crystal; Single crystal of (c) HOF-FJU-356 and (d) HOF-FJU-357 EIS test connection method

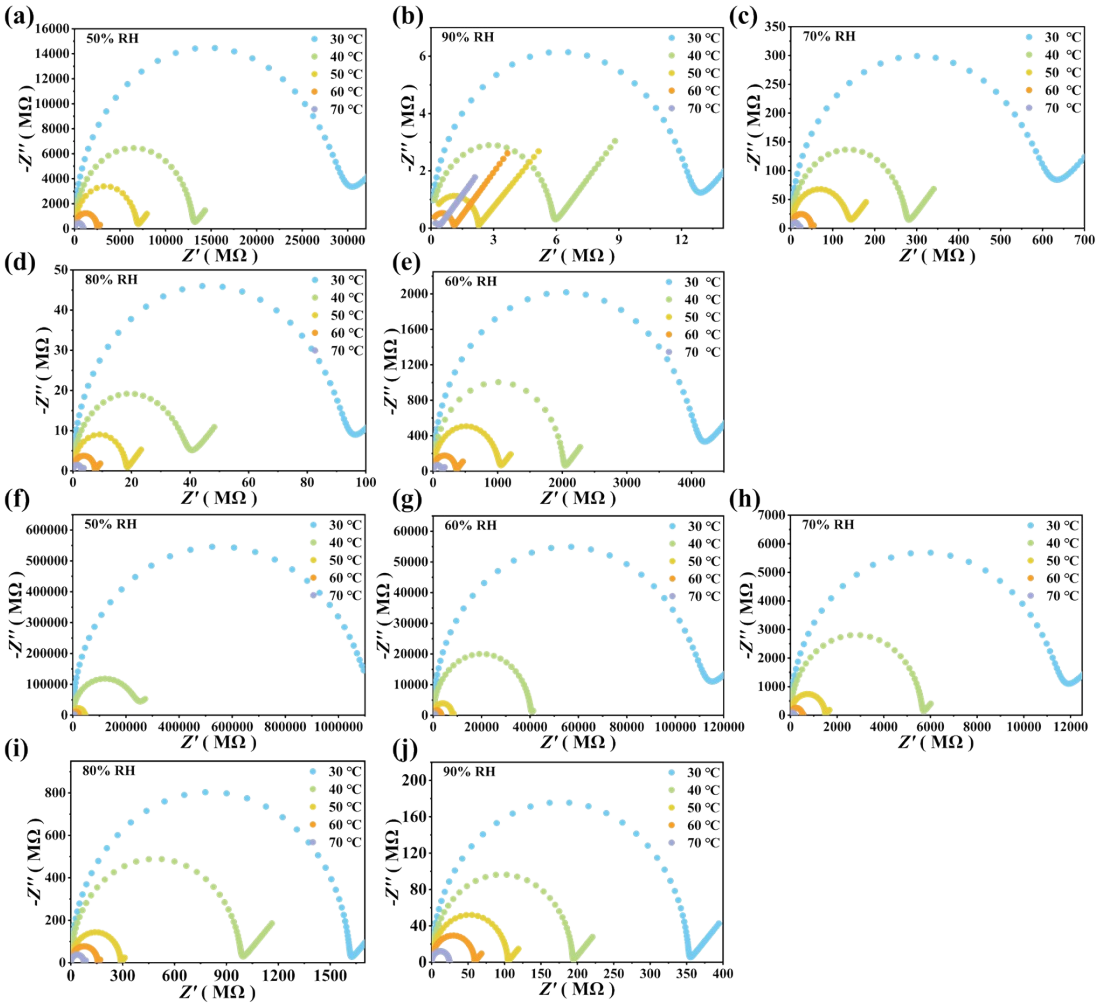

Fig. S6. (a-e) Single-crystal conductivity measurements of HOF-FJU-356 along the (0,1,0) direction at different relative humidities; (f–j) corresponding measurements of HOF-FJU-357 along the (1,0,0) direction.

Table S3. The proton conductivity (S cm^{-1}) of the HOF-FJU-356 single crystal along the (0,1,0) direction at temperatures ranging from 30 to 70 °C and under different relative humidities (RH).

RH	30 ℃	40 ℃	50 ℃	60 ℃	70 ℃
50%	2.40×10^{-8}	5.56×10^{-8}	1.05×10^{-7}	2.90×10^{-7}	7.68×10^{-7}
60%	1.63×10^{-7}	3.60×10^{-7}	6.98×10^{-7}	2.01×10^{-6}	5.13×10^{-6}
70%	1.14×10^{-6}	2.61×10^{-6}	5.02×10^{-6}	1.45×10^{-5}	3.60×10^{-5}
80%	7.60×10^{-6}	1.82×10^{-5}	3.92×10^{-5}	9.61×10^{-5}	2.47×10^{-4}
90%	5.69×10^{-5}	1.23×10^{-4}	3.19×10^{-4}	6.67×10^{-4}	1.81×10^{-3}
98%	3.67×10^{-4}	9.03×10^{-4}	2.33×10^{-3}	4.86×10^{-3}	1.22×10^{-2}

Table S4. The proton conductivity (S cm^{-1}) of the HOF-FJU-357 single crystal along the (1,0,0) direction at temperatures ranging from 30 to 70°C and under different relative humidities (RH)

RH	30 ℃	40 ℃	50 ℃	60 ℃	70 ℃
50%	8.49×10^{-9}	3.66×10^{-8}	2.04×10^{-7}	4.24×10^{-7}	1.45×10^{-6}
60%	8.04×10^{-8}	2.27×10^{-7}	1.15×10^{-6}	2.78×10^{-6}	9.99×10^{-6}
70%	7.77×10^{-7}	1.63×10^{-6}	6.13×10^{-6}	1.81×10^{-5}	5.17×10^{-5}
80%	5.68×10^{-6}	9.30×10^{-6}	3.19×10^{-5}	5.93×10^{-5}	1.22×10^{-4}
90%	2.61×10^{-5}	4.77×10^{-5}	8.81×10^{-5}	1.57×10^{-4}	3.81×10^{-4}
98%	1.14×10^{-4}	1.79×10^{-4}	2.92×10^{-4}	5.06×10^{-4}	1.12×10^{-3}

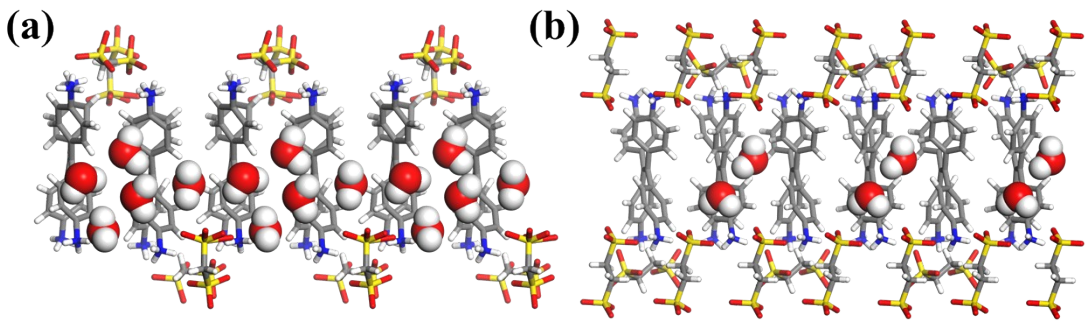

Fig. S7. Simulated distribution of water molecules within the pore channels of (a) HOF-FJU-356 and (b) HOF-FJU-357 under saturated adsorption conditions, showing an effectively continuous hydrogen-bonded network in HOF-FJU-356 and discrete water clusters in HOF-FJU-357.

Table S5. Comparison of proton conductivity for HOF-FJU-356/357 and other representative conductors. (SC: single crystal)

HOFs	Proton conductivity σ (S cm^{-1})	Sample form	Conditions (T, RH)	E_a (eV)	Ref
HOF-FJU-356	1.22×10^{-2}	[0,1,0]	70 ℃, 98% RH	0.806	This work
HOF-FJU-357	1.12×10^{-3}	[1,0,0]	70 ℃, 98% RH	0.529	This work
iHOF-3	1.67×10^{-3}	pellet	100 ℃, 98% RH	0.46/0.22	[4]
iHOF-4	2.76×10^{-3}	pellet	100 ℃, 98% RH	0.41	[4]
iHOF-16	5.56×10^{-3}	[0,1,0]	80 ℃, 98% RH	0.73	[5]
UPC-H5a@$NH_3 \cdot H_2O$	1.59×10^{-1}	pellet	80 ℃, 99% RH	0.4	[6]
UPC-H5a	3.42×10^{-2}	pellet	80 ℃, 99% RH	0.2	[6]
UPC-H5	1.85×10^{-3}	pellet	80 ℃, 99% RH	0.23	[6]
UPC-H3	9.00×10^{-2}	pellet	80 ℃, 99% RH	0.39	[7]
UPC-H2	6.90×10^{-3}	pellet	80 ℃, 99% RH	0.79	[7]
HOF-H3L	6.91×10^{-5}	pellet	100 ℃, 98% RH	0.68	[8]
[bpds][22bpy]	8.69×10^{-5}	pellet	90 ℃, 95% RH	0.51	[9]
[bpds][bpee]$\cdot 2H_2O$	1.09×10^{-3}	pellet	90 ℃, 95% RH	0.56	[9]
[bpds][bpdoz]$\cdot H_2O$	1.27×10^{-4}	pellet	90 ℃, 95% RH	0.43	[9]
GP-1	5.27×10^{-6}	pellet	80 ℃, 98% RH	0.35	[10]
GP-2	2.75×10^{-6}	pellet	80 ℃, 98% RH	0.46	[10]
IITKGP-HOF-1	5.29×10^{-2}	SC	80 ℃, 98% RH	0.52	[11]
IITKGP-HOF-3	7.6×10^{-6}	SC	80 ℃, 98% RH	0.42	[11]
iHOF-43	1.25×10^{-2}	Pellet	100 ℃, 98% RH	0.43	[12]
HOF-FJU-13	1.14×10^{-4}	[1,0,0]	60 ℃, 98% RH	0.72	[13]
HOF-FJU-12	1.54×10^{-5}	[1,0,0]	60 ℃, 98% RH	0.88	[13]
CPOS-1	1.0×10^{-2}	pellet	60 ℃, 98% RH	0.93	[14]
CPOS-2	2.2×10^{-2}	pellet	60 ℃, 98% RH	0.61	[14]
CPOS-3	3.3×10^{-4}	pellet	60 ℃, 98% RH	0.62	[14]
CPOS-4	7.4×10^{-4}	pellet	60 ℃, 98% RH	0.82	[14]
KUF-1a	1.53×10^{-3}	pellet	80 ℃, 98% RH	0.79	[15]

References

1. O. V. Dolomanov, L. J. Bourhis, R. J. Gildea, J. A. K. Howard and H. Puschmann, OLEX2: a complete structure solution, refinement and analysis program, *J. Appl. Crystallogr*, 2009, **42**, 339–341.
2. G. M. Sheldrick, *SHELXT* – Integrated space-group and crystal-structure determination, *Acta. Crystallogr. E*, 2015, **71**, 3–8.
3. S. Xu, X. Bai, J. Ma, M. Xu, G. Hu, T. D. James and L. Wang, Ultrasmall organic nanoparticles with aggregation-induced emission and enhanced quantum yield for fluorescence cell imaging, *Anal. Chem.*, 2016, **88**, 7853–7857.
4. X.-Q. Xu, L.-H. Cao, Y. Yang, F. Zhao, X.-T. Bai and S.-Q. Zang, Hybrid nafion membranes of ionic hydrogen-bonded organic framework materials for proton conduction and PEMFC applications, *ACS Appl. Mater. Interfaces*, 2021, **13**, 56566–56574.
5. X.-J. Cao, L.-H. Cao, X.-T. Bai, X.-Y. Hou and H.-Y. Li, An ultra-robust and 3d proton transport pathways iHOF with single-crystal superprotonic conductivity around 0.4 S cm^{-1}, *Adv. Funct. Mater.*, 2024, **34**, 2409359.
6. Y. Wang, J. Yin, D. Liu, C. Gao, Z. Kang, R. Wang, D. Sun and J. Jiang, Guest-tuned proton conductivity of a porphyrinylphosphonate-based hydrogen-bonded organic framework, *J. Mater. Chem. A*, 2021, **9**, 2683–2688.
7. Q. Yang, Y. Wang, Y. Shang, J. Du, J. Yin, D. Liu, Z. Kang, R. Wang, D. Sun and J. Jiang, Three hydrogen-bonded organic frameworks with water-induced single-crystal-to-single-crystal transformation and high proton conductivity, *Cryst. Growth Des.,* 2020, **20**, 3456–3465.
8. Z.-B. Sun, Y.-L. Li, Z.-H. Zhang, Z.-F. Li, B. Xiao and G. Li, A path to improve proton conductivity: from a 3D hydrogen-bonded organic framework to a 3D copper-organic framework, *New J. Chem.*, 2019, **43**, 10637–10644.
9. F.-W. Dong, Y.-L. Zhang, K.-H. Zhang, Y. Chen, A.-N. Sun and D. Shao, Proton conduction in three molecular assemblies of bipyridyl–organodisulfonate salts, *CrystEngComm*, 2025, **27**, 7850–7857.
10. F. Xiang, F. Lu, L. Li, Y. Lin, Y. Yang, Z. Zhang, J. Fu and S. Xiang, Solvent guest-induced guanidine organophosphonate inclusion complex for para-xylene encapsulation and proton conduction, *Cryst. Growth Des.*, 2026, **26**, 516–523.
11. S. Chand, W.-H. Deng, S. C. Pal, A. Saha, A. K. Manna and M. C. Das, Biomimetic water-stable multicomponent HOFs as ultrahigh superprotonic conductors, *ACS Energy Lett.*, 2026, **11**, 451–463.
12. S.-H. Li, L.-H. Cao, W. Zhang, X.-T. Bai and X.-Y. Chen, Multi-hydrophilic groups synergistic assembly ionic HOFs with multiple-water clusters and superprotonic single-crystal conductivity, *Chem. Commun.*, 2025, **61**, 4034–4037.
13. S. Zheng, L. Li, L. Chen, Z. Fan, F. Xiang, Y. Yang, Z. Zhang and S. Xiang, Two water stable phosphate-amidinium based hydrogen-bonded organic framework with proton conduction, *Z. Anorg. Allg. Chem.*, 2022, **648**, e202200031.
14. G. Xing, T. Yan, S. Das, T. Ben and S. Qiu, Synthesis of crystalline porous organic salts with high proton conductivity, *Angew. Chem. Int. Ed.*, 2018, **57**, 5345–5349.

15. D. W. Kang, M. Kang, H. Kim, J. H. Choe, D. W. Kim, J. R. Park, W. R. Lee, D. Moon, C. S. Hong, A hydrogen-bonded organic framework (HOF) with type IV NH_3 adsorption behavior, *Angew. Chem. Int. Ed.*, 2019, **58**, 16152–16155.